mathematics

MDPI

Article

Localized Boundary Knot Method for Solving Two-Dimensional Laplace and Bi-Harmonic Equations

Jingang Xiong, Jiancong Wen and Yan-Cheng Liu *

School of Civil Engineering and Architecture, Nanchang University, Nanchang 330031, China; xiongjingang@ncu.edu.cn (J.X.); wenjiancong95@163.com (J.W.)

* Correspondence: yanchengliu1113@gmail.com

Received: 30 June 2020; Accepted: 23 July 2020; Published: 24 July 2020

Abstract: In this paper, a localized boundary knot method is proposed, based on the local concept in the localized method of fundamental solutions. The localized boundary knot method is formed by combining the classical boundary knot method and the localization approach. The localized boundary knot method is truly free from mesh and numerical quadrature, so it has great potential for solving complicated engineering applications, such as multiply connected problems. In the proposed localized boundary knot method, both of the boundary nodes and interior nodes are required, and the algebraic equations at each node represent the satisfaction of the boundary condition or governing equation, which can be derived by using the boundary knot method at every subdomain. A sparse system of linear algebraic equations can be yielded using the proposed localized boundary knot method, which can greatly reduce the computer time and memory required in computer calculations. In this paper, several cases of simply connected domains and multi-connected domains of the Laplace equation and bi-harmonic equation are demonstrated to evidently verify the accuracy, convergence and stability of this proposed meshless method.

Keywords: localized meshless method; boundary knot method; sparse matrix; Laplace equation; bi-harmonic equation; multiply connected domain

1. Introduction

With the emergence of various engineering problems, an increasing number of numerical methods have been proposed in the past decades. To date, there are some well-known numerical methods, such as the finite difference method (FDM) [1,2], the finite element method (FEM) [3] and the boundary element method (BEM) [4]. These three methods are relatively mature, but they still have some obvious shortcomings and limitations. For example, with these methods, grid generation is difficult, especially for problems in complicated domains. They need to constantly remesh when calculating specific problems, which may result in high computational costs. On the contrary, there are some so-called meshless methods, which can solve problems without time-consuming mesh generation. From the present studies of meshless methods, it is evidently demonstrated that the meshless methods, proposed recently, are truly free from mesh and numerical quadrature, so they can be adopted to efficiently analyze physical problems and engineering applications with complex geometries.

In recent years, various meshless or meshfree numerical methods have been proposed to eliminate the time-consuming task of meshing. Meshless methods usually require node information only and do not need any orthogonal grid or unstructured mesh to acquire convergent, accurate and stable numerical solutions. These newly developed meshless methods have attracted the attention of many scholars [5]. Among them, the Radial basis function (RBF)-related method is the most popular, which

was proposed by Hardy [6]. Duchon [7] and Franke [8] successively proposed different algorithms to select the optimal parameters. The RBF collocation method (RBFCM), developed by Kansa [9,10] in 1990, allows RBFs to solve partial differential equations (PDEs). The RBFCM is an approximate expression that uses the RBF as the basis function to construct the numerical solution. The RBFCM has been developed to form the local RBFCM (LRBFCM), which can yield a sparse matrix, so the LRBFCM is applied to solve large-scale engineering science problems [11–15].

Another well-known meshless method is the method of fundamental solutions (MFS), which was first proposed by Kupradze and Aleksidze [16]. The MFS takes the fundamental solution as the basis function and is a special case of the Trefftz method [17]. The MFS require fictitious boundaries, which are called sources. The MFS only needs numerical calculations between boundary nodes and sources, and the homogeneous problems can be efficiently solved by discretization of boundary nodes only. However, in large-scale simulations, the conventional MFS cannot effectively and quickly solve problems in complex domains [18–20] owing to the fully populated coefficients matrix. In order to extend the MFS to large-scale problems, the localized MFS was proposed in 2019 by combining the MFS and the concept of localization. The localized method of fundamental solutions (LMFS) approximate the numerical solution by implementing the MFS within each local subdomain and the sparse system of linear algebraic equations of the LMFS can be efficiently solved even for problems in complicated domains. Recently, some researchers successfully used the LMFS to analyze the three-dimensional interior acoustic field [21]. Although the mathematical background of LMFS and the numerical implementation are simple, the determination of the fictitious boundary for sources is still a challenge in the LMFS [22,23].

In addition, the MFS in combination with RBF is sometimes applied for solving inhomogeneous problems [24] or nonlinear problems (with the Picard iteration method or the homotopy analysis method) [25]. Combining the advantages of RBF and MFS, the boundary knot method (BKM) was proposed by Chen [26] in 2002 to avoid the problem of fictitious boundary and singularity in the arrangement of fundamental solutions in the MFS. The BKM uses an RBF, which satisfies the governing equation and is a nonsingular general solution, to replace the fundamental solution of the MFS, in order to avoid the singularity of the fundamental solution and retain the advantages of the MFS. As a boundary-type RBF methodology, the BKM has been widely and successfully applied to solve various types of PDEs [26–30]. For many mathematical and physical problems, it is verified that the BKM can acquired highly accurate solutions, such as convection diffusion problems and Helmholtz [31], heat conduction in nonlinear functionally graded material [32], etc. However, the researchers also found that although the accuracy of the traditional BKM for two-dimensional and three-dimensional problems is relatively high, the interpolation matrix is a dense, ill-conditioned matrix, which may cause the instability of the numerical simulation.

In this study, we combined the BKM and the localization concept from the LMFS to form the localized BKM, which can yield a sparse system of linear algebraic equations instead of an ill-conditioned matrix. Moreover, the proposed localized BKM can efficiently and accurately analyze problems with complicated domains using limited computational time and computer memory. In this paper, the Laplace equation and the bi-harmonic equation were calculated by using localized BKM, and the effectiveness and accuracy of the proposed meshless method were verified by several numerical examples.

The organization of this paper is depicted as follows: The Laplace equation and the bi-harmonic equation are briefly introduced in Section 2. Section 3 presents the numerical procedures of the localized BKM, while in Section 4, the numerical results of the localized BKM are compared with analytical solutions to verify the merits of the proposed meshless method. Finally, some conclusions and remarks are drawn in Section 5.

2. Mathematical Formulation of Laplace and Bi-Harmonic Equations

In this study, the numerical procedures of the localized BKM was proposed to solve the two-dimensional boundary value problem, which are governed by Laplace and bi-harmonic equations, respectively. The governing equation of Laplace is demonstrated as follows:

$$\nabla^2 u(x, y) = 0, \ (x, y) \in \Omega, \tag{1}$$

where $\nabla^2 = \frac{\partial^2}{\partial x^2} + \frac{\partial^2}{\partial y^2}$ is the two-dimensional Laplacian, $u(x, y)$ is the unknown variable in the computational domain Ω, Γ^D and Γ^N denote the boundary segments with Dirichlet boundary conditions and the Neumann boundary condition:

$$\frac{\partial u}{\partial \boldsymbol{n}} = h(x, y), \ (x, y) \in \Gamma^N, \tag{2}$$

$$u = g(x, y), \ (x, y) \in \Gamma^D, \tag{3}$$

where $\boldsymbol{n} = \left(n_x, n_y\right)$ is the unit outward normal vector on the boundary and $h = (x, y)$ and $g = (x, y)$ are the given boundary conditions, respectively. The other boundary value problem is the bi-harmonic equation:

$$\nabla^4 u(x, y) = 0, \ (x, y) \in \Omega. \tag{4}$$

The Neumann boundary condition, Equation (2) and the Dirichlet boundary condition, Equation (3), should be simultaneously applied to all of the boundaries, since the bi-harmonic equation is a fourth-order PDE. In the next section, the numerical procedures of the proposed localized BKM will be clearly described.

3. Description of the Numerical Procedures of the Localized BKM

3.1. Laplace Equation

To describe the numerical procedures of the proposed localized BKM, for a two-dimensional Laplace equation, we required $N = n_i + n_{b1} + n_{b2}$ computational nodes, where n_i is the number of the nodes inside the computational domain, n_{b1} and n_{b2} are the points along the whole boundary, Γ^D and Γ^N. The schematic diagram of the computational nodes is displayed in Figure 1a.

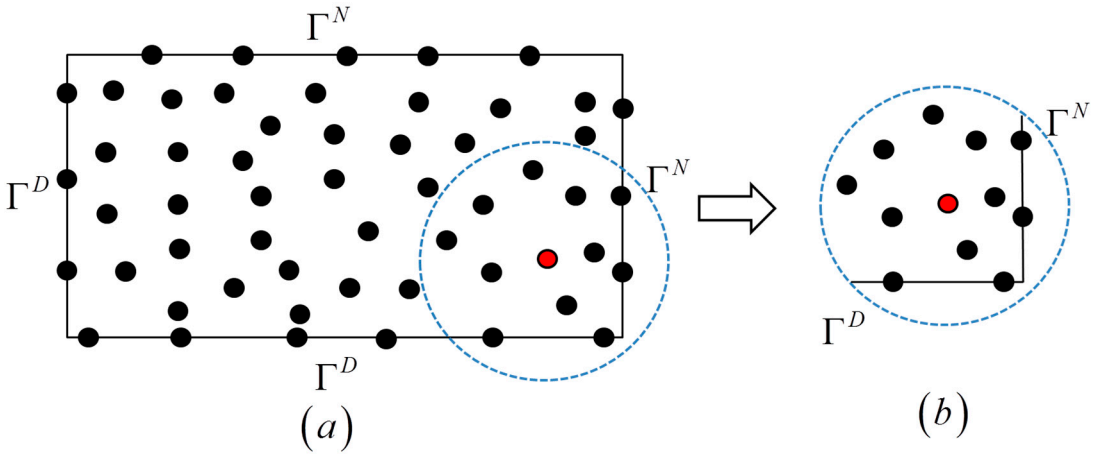

Figure 1. Schematic diagram for the computational domain. (***a***) Boundary and distribution of nodes and (***b***) subdomain.

To solve the two-dimensional boundary value problems, a subdomain, which is depicted in Figure 1b, will be formed for each node and the numerical solutions within each subdomain can be approximated by

$$u\left(x_j, y_j\right) = \sum_{s=1}^{N_s} \alpha_s \xi(r_s),\ x, y \in \Omega, \tag{5}$$

where N_s is the number of nodes in each subdomain. The determination of subdomain is identical to the LRBFCM, α_j^s are the unknown coefficients, $\boldsymbol{r} = \sqrt{\boldsymbol{x}^2 + \boldsymbol{y}^2}$, $\boldsymbol{x} = \parallel x - x_s \parallel$, $\boldsymbol{y} = \parallel y - y_s \parallel$, is the Euclidean distance and $\boldsymbol{x_s}$ represents the sth local node in the neighborhood of $\boldsymbol{x}$. The nonsingular general solution $\xi(\boldsymbol{x}, \boldsymbol{y}) = e^{(-c(x^2-y^2))}\cos(2c\boldsymbol{xy})$ satisfies the two-dimensional Laplace equation and is regular inside the computational domain. c is the shape parameter, which is adopted in the range $0 < c \leq 3$ in this paper.

From Equation (5)—and similarly to the LMFS [18–21]—the unknown coefficients $\boldsymbol{\alpha}_s^j$ can be transformed as follows:

$$\boldsymbol{\alpha}_s^j = \boldsymbol{\xi}_{N_s \times N_s}^{-1} \boldsymbol{u}_s^j, \tag{6}$$

where $\boldsymbol{u}_s = [u(x_1), \ldots, u(x_{N_s})]^T$, $\boldsymbol{\xi}_{N_s \times N_s}^{-1} = \left[\xi^{-1} \parallel x_j - x_i \parallel\right]^T$, $1 \leq i,\ j = N_s$. By substituting Equation (6) into Equation (1), the following expression can be derived:

$$\begin{aligned} Lu(x, y) &= \sum_{s=1}^{N_s} L\xi(\parallel x - x_s \parallel)\alpha_s = L\boldsymbol{\xi}_{N_s} \boldsymbol{\xi}_{N_s \times N_s}^{-1} \boldsymbol{u}_s^j \\ &= L\boldsymbol{\psi}_{1 \times N_s} \boldsymbol{u}_s^j = f(x, y), \end{aligned} \tag{7}$$

where L is the differential operator ∇^2, $\boldsymbol{\psi}_{1 \times N_s} = \boldsymbol{\xi}_{N_s} \boldsymbol{\xi}_{N_s \times N_s}^{-1}$, which is a vector with size $1 \times N_s$ and we use the MATLAB built-in command *pinv* to calculate $\boldsymbol{\xi}_{N_s \times N_s}^{-1}$, since $\boldsymbol{\xi}_{N_s \times N_s}^{-1}$ is an ill-conditioned matrix. Furthermore, from Equation (2), we have

$$\frac{\partial u^j}{\partial x} = \sum_{s=1}^{N_s} \alpha_s^j \frac{\partial}{\partial x} \xi \parallel x - x_s \parallel = \boldsymbol{\alpha}_s^j \frac{\partial \boldsymbol{\xi}_{N_s}}{\partial x} = \frac{\partial}{\partial x} \boldsymbol{\xi}_{N_s} \boldsymbol{\xi}_{N_s \times N_s}^{-1} \boldsymbol{u}_s^j = \boldsymbol{h}_s^{x(j)} \boldsymbol{u}_s^j,\ x \in \Gamma^N, \tag{8}$$

$$\frac{\partial u^j}{\partial y} = \sum_{s=1}^{N_s} \alpha_s^j \frac{\partial}{\partial y} \xi \parallel y - y_s \parallel = \boldsymbol{\alpha}_s^j \frac{\partial \boldsymbol{\xi}_{N_s}}{\partial y} = \frac{\partial}{\partial y} \boldsymbol{\xi}_{N_s} \boldsymbol{\xi}_{N_s \times N_s}^{-1} \boldsymbol{u}_s^j = \boldsymbol{h}_s^{y(j)} \boldsymbol{u}_s^j,\ y \in \Gamma^N. \tag{9}$$

In order to derive the expression for the Neumann boundary conditions, we can substitute Equations (8) and (9) into Equation (2):

$$\begin{aligned} \frac{\partial u}{\partial \boldsymbol{n}} &= \frac{\partial u}{\partial x} n_x + \frac{\partial u}{\partial y} n_y = \boldsymbol{h}_s^{x(j)} \boldsymbol{u}_s^j n_x + \boldsymbol{h}_s^{y(j)} \boldsymbol{u}_s^j n_y \\ &= B\boldsymbol{\psi}_{N_s} \boldsymbol{u}_s^j = h(x, y),\ x, y \in \Gamma^N, \end{aligned} \tag{10}$$

where

$$\begin{aligned} \boldsymbol{h}_s^{x(j)} &= \left[\frac{\partial \xi(r_1)}{\partial x}|_j \ \frac{\partial \xi(r_2)}{\partial x}|_j \ \cdots \ \frac{\partial \xi(r_s)}{\partial x}|_j\right]^T, \\ \boldsymbol{h}_s^{y(j)} &= \left[\frac{\partial \xi(r_1)}{\partial y}|_j \ \frac{\partial \xi(r_2)}{\partial y}|_j \ \cdots \ \frac{\partial \xi(r_s)}{\partial y}|_j\right]^T \end{aligned}$$

are the interpolation vectors of the discrete point satisfying the Neumann boundary conditions $\boldsymbol{\psi}_{N_s} = \boldsymbol{h}_s^{x(j)} n_x + \boldsymbol{h}_s^{y(j)} n_y$ and B are the differential operators in Γ^N. Equations (7) and (10) are the local forms, which is different from the global method. Now, we need to globalize this local form by inserting zero elements into the calculation. Therefore, Equations (7) and (10) can be transformed as follows:

$$Lu(x, y) = L\overline{\boldsymbol{\psi}}\overline{\boldsymbol{u}} = f(x, y),\ (x, y) \in \Omega, \tag{11}$$

$$Bu(x,y) = B\overline{\boldsymbol{\psi}}\overline{\boldsymbol{u}} = h(x,y),\ (x,y) \in \Gamma^N, \tag{12}$$

$$u(x,y) = \overline{\boldsymbol{\psi}}\overline{\boldsymbol{u}} = g(x,y),\ (x,y) \in \Gamma^D, \tag{13}$$

where $\overline{\boldsymbol{\psi}}(x,y) = \left[\overline{\psi}_1(x,y), \overline{\psi}_2(x,y), \ldots, \overline{\psi}_N(x,y)\right]$ is a sparse vector with the size of $1 \times N$, and N is the total number of nodes. All the values are zeros, except for the values obtained by interpolation at the corresponding positions of each discrete point in the local domain. Equation (13) represents the satisfaction of the Dirichlet boundary condition. The discretizations of the Laplace equation, the Neumann boundary condition and the Dirichlet boundary condition are combined to form a matrix as follows:

$$\boldsymbol{K} = \begin{bmatrix} \left(L\overline{\boldsymbol{\psi}}\right)_{n_i \times N} \\ \left(B\overline{\boldsymbol{\psi}}\right)_{n_{b2} \times N} \\ \left(\overline{\boldsymbol{\psi}}\right)_{n_{b1} \times N} \end{bmatrix}_{N \times N}, \boldsymbol{f} = \begin{bmatrix} f(x,y)_{n_i} \\ h(x,y)_{n_{b2}} \\ g(x,y)_{n_{b1}} \end{bmatrix},$$

$$\begin{aligned} \boldsymbol{K}\boldsymbol{u} &= \boldsymbol{f}, \\ \boldsymbol{u} &= \boldsymbol{K}^{-1}\boldsymbol{f}, \end{aligned} \tag{14}$$

where $\boldsymbol{K}_{N \times N}$ is the sparse coefficient matrix that avoids the ill-conditioned matrix, $\boldsymbol{u} = [u_1, u_2, \ldots, u_N]^T$ is the unknown field quantity and $\boldsymbol{f}$ is the given condition. Finally, $\boldsymbol{u}$ can be efficiently computed from Equation (14). From the descriptions of the numerical procedures, the proposed localized BKM, which is the combination of the conventional BKM and the localization concept from the LMFS and the LRBFCM, is very simple and easy to program. Furthermore, it can be expected that the localized BKM can be applied to engineering applications in complicated domains owing to the formation of a sparse system of linear algebraic equations.

3.2. Bi-Harmonic Equation

The numerical procedures of the proposed localized LBKM for solving the two-dimensional bi-harmonic equation are presented in this subsection. The numerical procedures of the localized BKM for solving the bi-harmonic equation is similar to the procedures for the Laplace equation described above. As compared with the Laplace equation, the bi-harmonic equation is a fourth-order PDE. In addition to the bi-harmonic equation, there are two boundary conditions, which should be imposed along the whole boundary at the same time. The process of the calculation is basically the same as that for the Laplace equation. The numerical solution within the local domain of the jth node can be represented as follows:

$$u^{(j)}(x,y) = \sum_{s=1}^{N_s} \alpha_s^j \xi(r) + \sum_{s=1}^{N_s} \beta_s^j r^2 \xi(r), \tag{15}$$

where $\boldsymbol{\alpha}_s^j$ and $\boldsymbol{\beta}_s^j$ are the unknown coefficients, and N_s is the number of nodes in the subdomain. For simplicity, Equation (15) can be simply transformed as follows:

$$\boldsymbol{u}^{(j)} = \boldsymbol{C}\boldsymbol{\omega}^{(j)}, \tag{16}$$

where $\boldsymbol{C}$ is the coefficient matrix based on the jth point and the neighboring N_s points through interpolation. $\boldsymbol{\omega} = [\alpha_1, \alpha_2, \ldots, \alpha_{N_s}, \beta_1, \beta_2, \ldots, \beta_{N_s}]^T$ is the vector of unknown coefficients. Similarly, from Equations (7)–(9), we can reformulate the governing equation and the boundary conditions as follows:

$$u^{(j)}(x,y) = \sum_{s=1}^{N_s} \alpha_s^j \xi(r) + \sum_{s=1}^{N_s} \beta_s^j r^2 \xi(r) = \boldsymbol{\eta}_{n_s}^{(j)} \boldsymbol{u}_{n_s}^{(j)},\ n_s = 1, 2, \ldots, N_s, \tag{17}$$

$$\frac{\partial u^j}{\partial x} = \sum_{s=1}^{N_s} \alpha_s^j \frac{\partial}{\partial x} \xi(r) + \sum_{s=1}^{N_s} \beta_s^j \frac{\partial}{\partial x} r^2 \xi(r) = \boldsymbol{\eta}_{n_s}^{x(j)} \boldsymbol{u}_{n_s}^{(j)}, \tag{18}$$

$$\frac{\partial u^j}{\partial y} = \sum_{s=1}^{N_s} \alpha_s^j \frac{\partial}{\partial y}\xi(r) + \sum_{s=1}^{N_s} \beta_s^j \frac{\partial}{\partial y} r^2 \xi(r) = \boldsymbol{\eta}_{n_s}^{y(j)} \boldsymbol{u}_{n_s}^{(j)}, \tag{19}$$

where $\boldsymbol{\eta}_{n_s}^{(j)}$, $\boldsymbol{\eta}_{n_s}^{x(j)}$ and $\boldsymbol{\eta}_{n_s}^{y(j)}$ are the weighting coefficients. The satisfaction of the governing equation is imposed at every interior node while the satisfactions of both boundary conditions, Equations (17)–(19), are enforced at each boundary node.

$$u^{(j)} - \boldsymbol{\eta}_{n_s}^{(j)} \boldsymbol{u}_{n_s}^{(j)} = 0, \; j = 1, 2, \ldots, n_i, \tag{20}$$

$$\begin{gathered} \frac{\partial u^{(j)}}{\partial n} = n_x^{(j)} \frac{\partial u^{(j)}}{\partial x} + n_y^{(j)} \frac{\partial u^{(j)}}{\partial y} = n_x^{(j)} \boldsymbol{\eta}_{n_s}^{x(j)} \boldsymbol{u}_{n_s}^{(j)} + n_y^{(j)} \boldsymbol{\eta}_{n_s}^{y(j)} \boldsymbol{u}_{n_s}^{(j)} = \boldsymbol{g}^{(j)}, \\ j = n_i + 1, n_i + 2, \ldots, n_i + n_b, \end{gathered} \tag{21}$$

$$u^{(j)} = g^{(j)}, \; j = n_i + n_b + 1, \ldots, n_i + 2n_b. \tag{22}$$

To combine Equations (20)–(22), we can acquire a matrix form of the linear algebraic equation

$$\boldsymbol{K}\boldsymbol{u} = \boldsymbol{f},$$

where $\boldsymbol{K}$ is the matrix with the size $(n_i + 2n_b) \times (n_i + n_b)$. Once the above system is accurately solved, the numerical solution of the proposed localized BKM can be obtained. However, it is also known that the numerical solutions may not be accurate enough as a result of the overdetermined system. In order to acquire a highly accurate solution, we adopted the ghost nodes, which is shown in Figure 2. As shown in Figure 2, we place a circle of ghost nodes around the boundary nodes and the distance between the ghost nodes and the boundary nodes is 1/2 the distance between the adjacent boundary nodes. When the base nodes are interpolated with its adjacent n_s, the adjacent ghost nodes are also selected to participate in the interpolation calculation. When $\boldsymbol{K}$ is calculated in this way, we can obtain a square coefficient matrix and an extremely accurate solution.

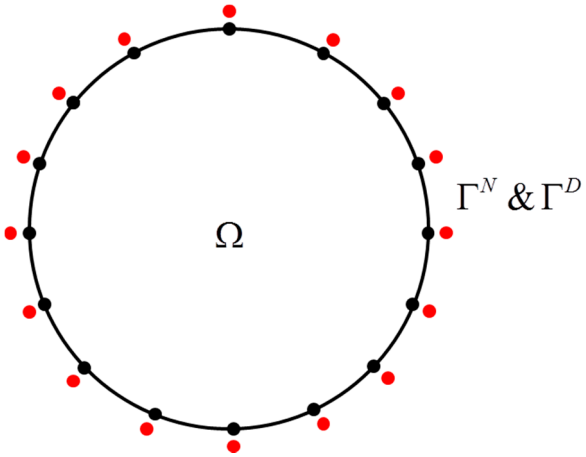

Figure 2. Schematic diagram of the ghost nodes arrangement.

4. Numerical Results and Comparisons

In this section, six numerical cases are given and the numerical results of the LBKM are compared. In order to prove the accuracy of the proposed algorithm, the simply connected domain and multi-connected domain are calculated and analyzed by changing the parameters, such as the shape parameters, the total number of nodes or the number of subdomains. Finally, the calculated

numerical solution u_n is compared with the analytical solution u_e, and the maximum absolute error is compared as an index. The calculation formula is as follows:

$$Abs\_error = \max_{1 \le j \le N} (|u_e^j - u_n^j|).$$

4.1. Case 1

In this case, we test a square domain, whose four boundaries are applied to the Dirichlet boundary conditions. A detailed diagram of the computational domain and the applied boundary conditions are shown in Figure 3. The analytical solution of the applied boundary condition is as follows:

$$u_e(x, y) = e^x \cos(y) + e^y \sin(x),$$

in which the corner points are removed from this computational domain, and the interior and boundary point are evenly distributed. Here, the parameters of calculation are given by

$$N = 10197,\ n_b = 396,\ n_s = 9,\ c = 0.1$$

where N is the total nodes, n_b is the boundary nodes, n_s is the number of subdomains, and c is the shape parameter. The maximum absolute error is 5.3892×10^{-5}, which can preliminarily prove the accuracy of LBKM. The distribution of the numerical solution is shown in Figure 4.

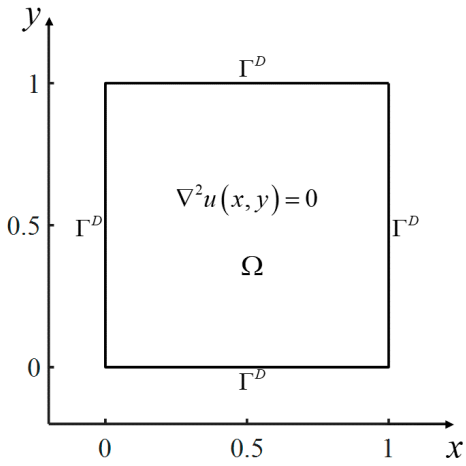

Figure 3. Schematic diagram of computational domain in Case 1.

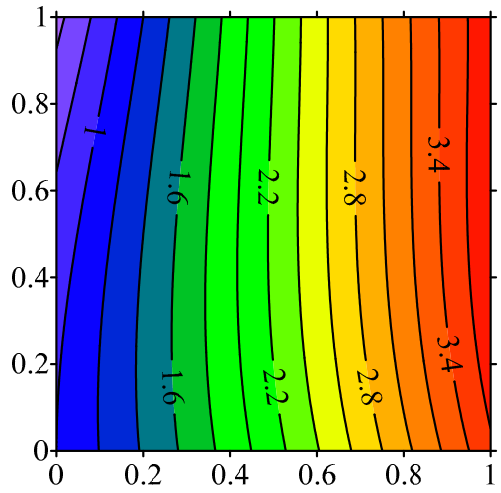

Figure 4. TDdistribution of numerical solutions in Case 1.

To verify the stability of the LBKM, we changed the number of boundary nodes and interior nodes at the same time. As can be seen in the results shown in Table 1, the results calculated using different parameters are considerable, the shape parameter c remains unchanged, and the maximum absolute error is 8.7091×10^{-6} when the total number of nodes reaches $N = 62997$.

Table 1. The maximum absolute error for Case 1.

N	**3717**	**6557**	**10,197**	**22,797**	**62,997**
n_b	236	316	396	596	996
n_s	9	9	9	9	9
Max error	1.1660×10^{-4}	8.3856×10^{-5}	5.3892×10^{-5}	1.9058×10^{-5}	8.7091×10^{-6}

4.2. Case 2

In order to further verify the impact of geometric complexity on the precision of the algorithm. In this case, a multiply connected domain is adopted as the computational domain. As shown in Figure 5, we apply Dirichlet boundary conditions and Neumann boundary conditions on each boundary, respectively. Here, the analytical solutions of the applied Dirichlet boundary conditions are as follows:

$$u_e(x, y) = x^2 - y^2 + xy + 2.$$

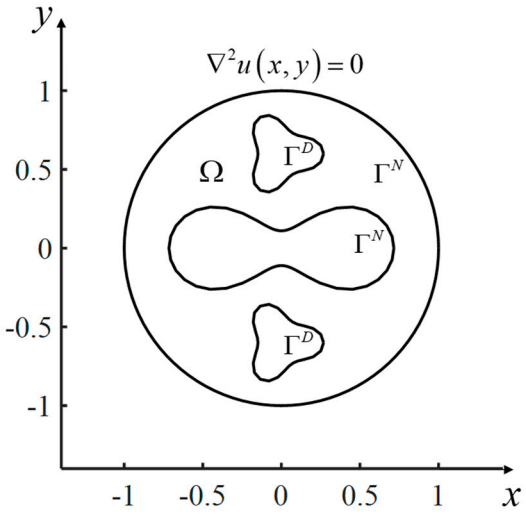

Figure 5. Schematic diagram of computational domain in Case 2.

In this case, the shape parameter is $c = 0.2$. The maximum absolute error can reach 5.1431×10^{-4}, when the total number of nodes is $N = 6762$, the boundary number is $n_b = 220$, and the number of the nodes in the local domain is 29. Figure 6 shows the distribution of the numerical solution. In addition, the results computed by different parameters are shown in Table 2. It can be seen that when the number of nodes in the computational domain increases slowly and the number of nodes in the subdomain changes, the results of the calculation are convergent. Therefore, the error of LBKM can reach the accuracy requirement when calculating the multi-domain.

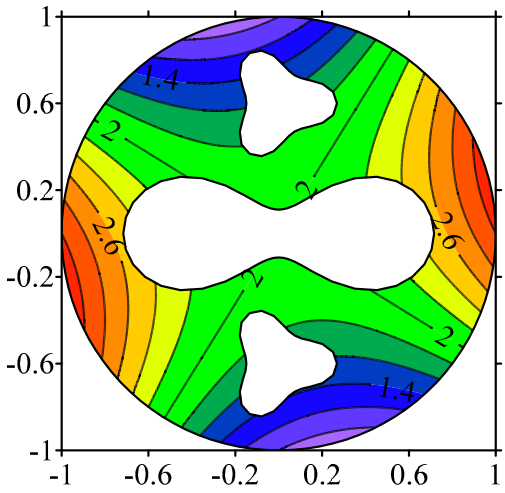

Figure 6. The distribution of numerical solution in Case 2.

Table 2. The maximum absolute error for Case 2.

N	1472	3286	6762	10,418	28,020
n_b	220	220	220	220	220
n_s	16	21	29	31	51
Max error	6.3997×10^{-3}	1.1289×10^{-3}	5.1431×10^{-4}	4.9134×10^{-4}	2.4991×10^{-4}

4.3. Case 3

For the third case, we simulate a simple connected domain to verify the accuracy of the solutions for the Laplace problem with non-harmonic boundary conditions. Furthermore, the analytic solution that we have is

$$u_e(x, y) = x^2 y^3 + 1,$$

which does not satisfy the Laplace equation. Figure 7 shows the schematic diagram of the computational domain. Table 3 shows the maximum absolute error for case 3. It can be seen from Table 3 that when the total number of nodes increases and the number of nodes in the local domain changes, the calculated result is convergent. When the total number of nodes is $N = 25064$, the number of boundary nodes is $n_b = 600$, the number of subdomain nodes $n_s = 18$, and the shape parameter is $c = 1$, the maximum absolute error is 5.2868×10^{-5}.

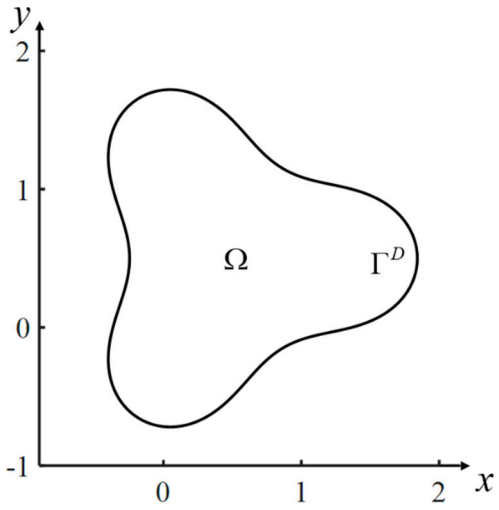

Figure 7. Schematic diagram of the computational domain in case 3.

Table 3. Maximum absolute error for case 3.

N	1256	4319	9385	16,269	25,064
n_b	150	250	400	500	600
n_s	9	9	12	15	18
Max error	8.0516×10^{-4}	9.1815×10^{-5}	1.0468×10^{-4}	7.9568×10^{-5}	5.2868×10^{-5}

In the above three cases, the new LBKM is used to solve the boundary value problem with the interior nodes satisfying the Laplace equation. By changing the total number of nodes N, the number of nodes n_s in local domain and the shape parameter c, the convergence of the results is obtained when calculating the simply connected domain and the multi-connected domain, respectively, which preliminarily verifies the accuracy of the algorithm. In the cases below, the bi-harmonic equations are tested to further verify the stability and accuracy of the method.

4.4. Case 4

In this case, we make a simulation of a governed bi-harmonic equation with two types of boundary conditions. There are two tests in this case. The calculation domain is shown in Figure 8.

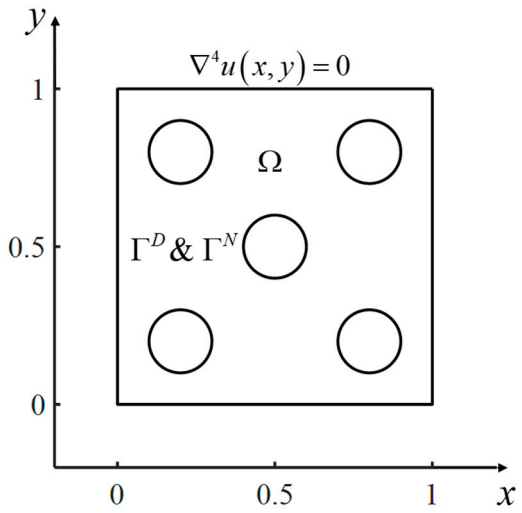

Figure 8. Schematic diagram of computational domain in case 4.

For the first test, the analytic solution we use is

$$u_e(x,y) = x^4 + y^4 - 6x^2y^2 + 3,$$

which satisfies both the Laplace equation and the bi-harmonic equation. Table 4 shows the results calculated with different parameters. The maximum absolute error is 1.7719×10^{-4} when the total number of nodes is $N = 2336$, the number of boundary nodes is $n_b = 296$, the number of local domain nodes is $n_s = 41$, and the shape parameter is $c = 3$. The distribution of the numerical solution is shown in Figure 9.

Table 4. Maximum absolute error for test 1 in case 4.

N	476	2336	5734	10,594	24,896
n_b	176	296	466	586	776
n_s	25	41	61	111	191
Max error	2.3232×10^{-4}	1.7719×10^{-4}	1.0121×10^{-4}	3.6471×10^{-4}	5.0082×10^{-4}

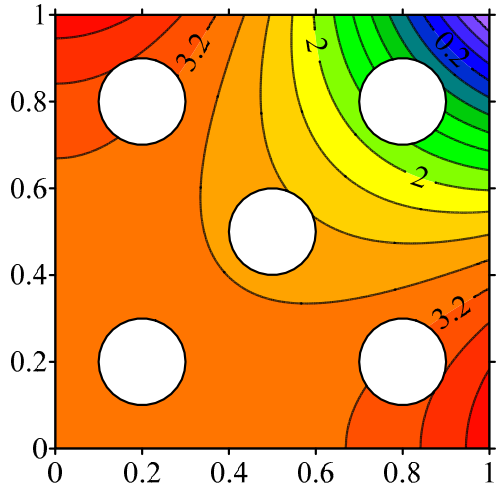

Figure 9. Distribution of the numerical solution for test 1 in case 4.

The other test uses the same computational domain and the same boundary conditions. However, the boundary condition can be calculated from the analytical solution as follows:

$$u_e(r,\theta) = r^{(-n+2)}sin(n\theta),\ n \geq 3,\ 0 \leq \theta \leq 2\pi,$$

where $r = \sqrt{x^2+y^2}$ is the Euclidean distance. The origin of the cylindrical coordinate (r_s, θ_s) is located at $(x, y) = (8, -4)$; Table 5 shows the maximum absolute error for this test. The distribution of the numerical solution is shown in Figure 10 for when the total number of nodes $N = 24896$, the number of boundary nodes $n_b = 776$, the number of nodes in the subdomain $n_s = 26$, and the shape parameter is $c = 1$.

Table 5. Maximum absolute error for test 2 in case 4.

N	**2336**	**4396**	**8776**	**12,536**	**24,896**
n_b	296	376	496	576	776
n_s	9	21	22	25	26
Max error	2.3931×10^{-4}	1.7264×10^{-4}	1.7978×10^{-4}	1.6569×10^{-4}	1.4221×10^{-4}

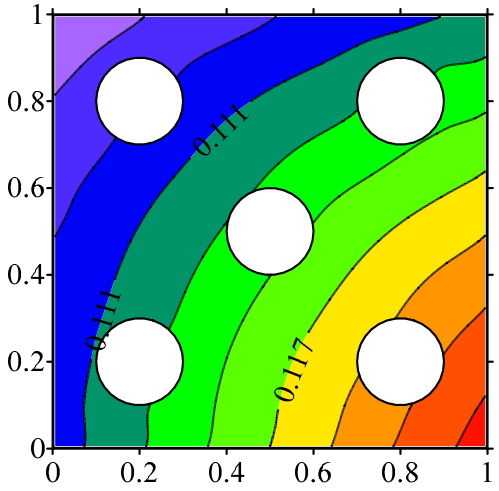

Figure 10. Distribution of the numerical solution for test 2 in case 4.

4.5. Case 5

In the fifth case, a multi-connected domain is considered. The computational domain is a square domain with a small square domain dug out, as shown in Figure 11.

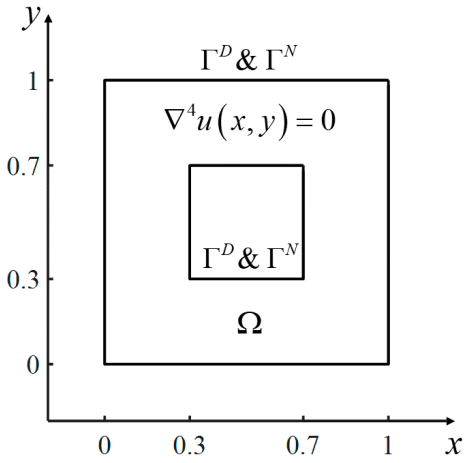

Figure 11. Schematic diagram of the computational domain in case 5.

The analytical solution is as follows:

$$u_e(x,y) = \frac{1}{2}x[\cos(x)\sinh(y) + \sin(x)\cosh(y)] + 1,$$

which only satisfies the bi-harmonic equation, but not the Laplace equation. The shape parameter in this case is $c = 0.5$. When the parameters are taken as follows: $N = 14552$, $n_b = 720$, $n_s = 49$, the maximum absolute error is 1.0615×10^{-3}. Table 6 shows the results for when we change the number of total nodes, N, and the number of different nodes in the subdomain, ns. We can see from Table 6 that the result converges and when the total number of nodes is $N = 27712$, the number of boundary nodes is $n_b = 1000$ and $n_s = 65$, the error can reach 9.7262×10^{-4}. Figure 12 is the distribution of the numerical solution.

Table 6. Maximum absolute error for case 5.

N	**832**	**3184**	**8672**	**14,552**	**27,712**
n_b	160	328	552	720	1000
n_s	9	18	29	49	65
Max error	1.5560×10^{-3}	1.4743×10^{-3}	1.0121×10^{-3}	1.0615×10^{-3}	9.7262×10^{-4}

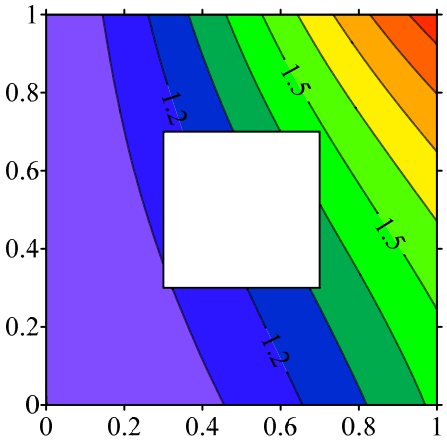

Figure 12. Distribution of the numerical solution in case 5.

4.6. Case 6

In the last case, we use the non-harmonic boundary conditions, governed by the bi-harmonic equation. Figure 13 shows the computational domain and the applied boundary conditions. The analytical solution we use is as follows:

$$u_e(x, y) = x^3 y^4 + 1.$$

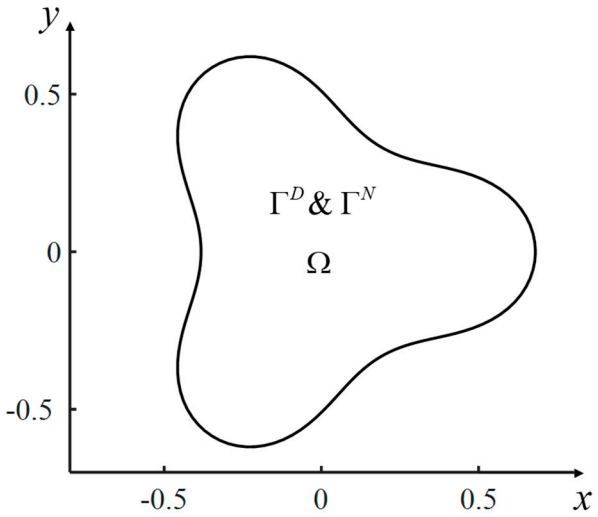

Figure 13. Schematic diagram of computational domain in case 6.

In this case, the shape parameter $c = 0.3$ is used. Since the non-harmonic is mainly affected by the boundary nodes, the number of nodes in the interior nodes and local domain remains unchanged, only the number of boundary nodes is changed. Table 7 shows the numerical results calculated at different boundary nodes.

Table 7. Maximum absolute error for case 6.

N	**2240**	**2346**	**2446**	**2546**	**2646**
nb	50	100	150	200	250
ns	31	31	31	31	31
Max error	3.1994×10^{-4}	1.5152×10^{-4}	1.0441×10^{-4}	5.8681×10^{-5}	2.1867×10^{-5}

5. Conclusions

In this paper, the localized BKM is proposed to solve two-dimensional Laplace and bi-harmonic equations accurately and efficiently. The proposed meshless method is the combination of the convectional BKM and the concept of localization from the LMFS and the LRBFCM. The proposed method is truly free from time-consuming mesh generation and numerical quadrature since only a set of randomly distributed nodes are required for the numerical simulation. Furthermore, the troublesome problems of determination of the fictitious boundary for sources can be simply avoided by using the nonsingular general solution. Since the resultant system of algebraic equations is sparse, it can be expected that the proposed localized BKM can be used to solve realistic engineering applications in complicated domains.

In this paper, six numerical examples are provided to demonstrate the merits of the proposed localized BKM. According to the numerical results and comparisons, the following conclusions can be drawn:

(1) In this paper, a novel meshless method, the localized BKM, is proposed to accurately and efficiently solve two-dimensional Laplace and bi-harmonic equations;
(2) As a result of the use of localization, the resultant system of algebraic equations is sparse, so it is evident that the proposed localized BKM is capable of efficiently solving large-scale problems;
(3) As compared with the MFS, the RBFCM and other meshless methods, the problems of ill-conditioned matrix and the determination of the fictitious boundary for sources are avoided in the proposed method;
(4) In the examples provided, it is evident that the proposed localized BKM can accurately solve problems in simply connected and multiply connected domains. Furthermore, both the Laplace equation with a non-harmonic condition and the bi-harmonic equation with a non-bi-harmonic conditions can be stably analyzed by the proposed meshless method.

In the future, the proposed localized BKM will be improved and extended to analyze various physical and mathematical problems, such as temporal transient problems, inverse problems, the acoustic problem, the moving-boundary problem, three-dimensional problems, etc.

Author Contributions: Supervision, J.X.; Formal analysis, Software, Validation and Writing—original draft preparation, J.W.; Conceptualization, Data curation, Project administration and Writing—review & editing. Y.-C.L.; All authors have read and agreed to the published version of the manuscript.

Funding: This research received no external funding.

Conflicts of Interest: The authors declare no conflict of interest.

References

1. Liszka, T.; Orkisz, J. The finite difference method at arbitrary irregular grids and its application in applied mechanics. *Comput. Struct.* **1980**, *11*, 83–95. [CrossRef]
2. Vachiratienchai, C.; Boonchaisuk, S.; Siripunvaraporn, W. A hybrid finite difference–Finite element method to incorporate topography for 2D direct current (DC) resistivity modeling. *Phys. Earth Planet. Inter.* **2010**, *183*, 426–434. [CrossRef]
3. Solberg, J.M.; Papadopoulos, P. A finite element method for contact/impact. *Finite Elem. Anal. Des.* **1998**, *30*, 297–311. [CrossRef]
4. Brebbia, C.A. *The Boundary Element Method for Engineers*; Pentech Press: Plymouth, UK, 1978.
5. Xia, P.; Long, S.; Wei, K. The dynamic analysis for the non-Homogeneous modeately thick plate by the meshless LRPIM. *Chin. J. Comput. Mech.* **2010**, *27*, 1029–1035.
6. Hardy, R.L. Multiquadric equations of topography and other irregular surfaces. *J. Geophys. Res.* **1971**, *76*, 1905–1915. [CrossRef]
7. Duchon, J. Splines Minimizing Rotation-Invariant Semi-Norms in Sobolev Spaces. In *Constructive Theory of Functions of Several Variables*; Springer: Berlin, Germany, 1977; pp. 85–100.
8. Franke, R. Scattered data interpolation: Tests of some methods. *Math. Comput.* **1982**, *38*, 181–200.
9. Kansa, E.J. Multiquadrics—A scattered data approximation scheme with applications to computational fluid-dynamics—II solutions to parabolic, hyperbolic and elliptic partial differential equations. *Comput. Math. Appl.* **1990**, *19*, 147–161. [CrossRef]
10. Kansa, E.J. Multiquadrics—A scattered data approximation scheme with applications to computational fluid-Dynamics—I surface approximations and partial derivative estimates. *Comput. Math. Appl.* **1990**, *19*, 127–145. [CrossRef]
11. Zheng, H.; Zhang, C.Z.; Wang, Y.S.; Sladek, J.; Sladek, V. A meshfree local RBF collocation method for anti-Plane transverse elastic wave propagation analysis in 2D phononic crystals. *J. Comput. Phys.* **2016**, *305*, 997–1014. [CrossRef]
12. Zheng, H.; Zhang, C.Z.; Wang, Y.S.; Sladek, J.; Sladek, V. Band structure computation of in-Plane elastic waves in 2D phononic crystals by a meshfree local RBF collocation method. *Eng. Anal. Bound. Elem.* **2016**, *66*, 77–90. [CrossRef]
13. Zheng, H.; Yao, G.M.; Lei, H.K.; Li, X.X. On the selection of a good shape parameter of localized method of approximated particular solutions. *Adv. Appl. Math. Mech.* **2018**, *10*, 1–16. [CrossRef]

14. Zheng, H.; Yang, Z.; Zhang, C.; Tyrer, M. A local radial basis function collocation method for band structure computation of phononic crystals with scatterers of arbitrary geometry. *Appl. Math. Model.* **2018**, *60*, 447–459. [CrossRef]
15. Zheng, H.; Xiong, J.G.; Yuan, Y.; Wen, P.H. Mixed-Mode dynamic stress intensity factors by variation technique with finite block method. *Eng. Anal. Bound. Elem.* **2019**, *106*, 27–33. [CrossRef]
16. Kupradze, V.D.; Aleksidze, M.A. The method of functional equations for the approximate solution of certain boundary value problems. *USSR Comput. Math. Math. Phys.* **1964**, *4*, 82–126. [CrossRef]
17. Kołodziej, J.A.; Grabski, J.K. Many names of the Trefftz method. *Eng. Anal. Bound. Elem.* **2018**, *96*, 169–178. [CrossRef]
18. Fan, C.M.; Huang, Y.K.; Chen, C.S. Localized method of fundamental solutions for solving two-Dimensional Laplace and bi-harmonic equations. *Eng. Anal. Bound. Elem.* **2019**, *101*, 188–197. [CrossRef]
19. Gu, Y.; Fan, C.M.; Qu, W.Z. Localized method of fundamental solutions for large-Scale modelling of three-Dimensional anisotropic heat conduction problems–Theory and MATLAB code. *Comput. Struct.* **2019**, *220*, 144–155. [CrossRef]
20. Gu, Y.; Fan, C.M.; Xu, R.P. Localized method of fundamental solutions for large-Scale modeling of two-Dimensional elasticity problems. *Appl. Math. Lett.* **2019**, *93*, 8–14. [CrossRef]
21. Qu, W.; Fan, C.M.; Gu, Y.; Wang, F. Analysis of three-Dimensional interior acoustic fields by using the localized method of fundamental solutions. *Appl. Math. Model.* **2019**, *76*, 122–132. [CrossRef]
22. Wang, F.; Liu, C.S.; Qu, W. Optimal sources in the MFS by minimizing a new merit function: Energy gap functional. *Appl. Math. Lett.* **2018**, *86*, 229–235. [CrossRef]
23. Liu, C.S.; Wang, F. An energy method of fundamental solutions for solving the inverse Cauchy problems of the Laplace equation. *Comput. Math. Appl.* **2018**, *75*, 4405–4413. [CrossRef]
24. Golberg, M.A. The method of fundamental solutions for Poisson's equation. *Eng. Anal. Bound. Elem.* **1995**, *16*, 205–213. [CrossRef]
25. Uscilowska, A. The MFS as a basis for the PIM or the HAM–Comparison of numerical methods. *Eng. Anal. Bound. Elem.* **2015**, *57*, 72–87. [CrossRef]
26. Chen, W.; Tanaka, M. A meshless, integration-Free, and boundary-Only RBF technique. *Comput. Math. Appl.* **2002**, *43*, 379–391. [CrossRef]
27. Chen, W.; Hon, Y.C. Numerical investigation on convergence of boundary knot method in the analysis of homogeneous Helmholtz, modified Helmholtz, and convection–Diffusion problems. *Comput. Methods Appl. Mech. Eng.* **2003**, *192*, 1859–1875. [CrossRef]
28. Jin, B.; Zheng, Y. Boundary knot method for some inverse problems associated with the Helmholtz equation. *Int. J. Numer. Methods Eng.* **2005**, *62*, 1636–1651. [CrossRef]
29. Jin, B.; Chen, W. Boundary knot method based on geodesic distance for anisotropic problems. *J. Comput. Phys.* **2006**, *215*, 614–629. [CrossRef]
30. Jiang, X.; Chen, W.; Chen, C.S. Fast multipole accelerated boundary knot method for inhomogeneous Helmholtz problems. *Eng. Anal. Bound. Elem.* **2013**, *37*, 1239–1243. [CrossRef]
31. Hon, Y.C.; Chen, W. Boundary knot method for 2D and 3D Helmholtz and convection–Diffusion problems under complicated geometry. *Int. J. Numer. Methods Eng.* **2003**, *56*, 1931–1948. [CrossRef]
32. Fu, Z.J.; Chen, W.; Qin, Q.H. Boundary knot method for heat conduction in nonlinear functionally graded material. *Eng. Anal. Bound. Elem.* **2011**, *35*, 729–734. [CrossRef]